Rock Mech Rock Eng (2017) 50:871–889
DOI 10.1007/s00603-016-1137-3

ORIGINAL PAPER

Poroelasticity of the Callovo–Oxfordian Claystone

Malik Belmokhtar[1] · Pierre Delage[1] · Siavash Ghabezloo[1] · Anh-Minh Tang[1] · Hamza Menaceur[1,3] · Nathalie Conil[2]

Received: 1 April 2016 / Accepted: 17 November 2016 / Published online: 25 November 2016

Abstract This work is devoted to an experimental investigation of the poroelastic behavior of the Callovo–Oxfordian claystone, a potential host rock for the deep underground repository of high-level radioactive waste in France. Drained, undrained, pore pressure loading and unjacketed tests were carried out in a specially designed isotropic compression cell to determine the poroelastic parameters of fully saturated specimens. Great care was devoted to the saturation procedure, and small loading rates were used to ensure full drainage conditions in drained and pore pressure tests (0.5 kPa/min) and in the unjacketed test (2 kPa/min). High-precision strain measurements were performed by ensuring direct contact between the LVDT stems and the specimen. An analysis in the framework of transverse isotropic poroelasticity provided the Biot effective stress coefficients b_1 (perpendicular to bedding) between 0.85 and 0.87 and b_2 (parallel to bedding) between 0.90 and 0.98 under different stress conditions (pore pressure 4 MPa, total isotropic stresses of 14 and 12 MPa, respectively). A set of equivalent isotropic poroelastic parameters was also determined and a very good compatibility between the results of different tests was found, giving confidence in the parameters determined. The unjacketed test provided a directly reliable measurement of the unjacketed modulus ($K_s = 21.7$ GPa) that was afterward confirmed by an indirect evaluation that showed the non-dependency of K_s with respect to the stress level. These parameters were obtained for specimens cored and trimmed in the laboratory. A parametric study was then conducted so as to provide an estimation of the parameters in situ, i.e., not submitted to the damage supported by laboratory specimens. A minimal value $b = 0.77$ seems to be a reasonable lower bound for the equivalent isotropic Biot parameter.

Keywords Claystone · Isotropic compression cell · Poroelasticity · Transverse isotropy · Biot coefficients · Unjacketed modulus

1 Introduction

A possible host rock for geological radioactive waste disposal in France is the Callovo–Oxfordian (COx) claystone, a sedimentary clayey rock from the Paris basin deposited 155 million years ago into a 150-m-thick layer slightly tilting with an inclination of 2° with respect to horizontal over a layer of Dogger limestone and covered by a layer of Oxfordian limestone. Detailed investigations on the properties of the COx claystone are carried out in the Underground Research Laboratory (URL) managed by Andra, the French agency for the management of radioactive waste, close to the village of Bure in Eastern France. The URL is located at a depth of 490 m, at which the clay fraction in the claystone is maximum and close to 50%. A detailed investigation of the in situ state of stress in the Bure URL was conducted by Wileveau et al. (2007), providing the following stress values: vertical total stress $\sigma_V = 12.7$ MPa (lithostatic), major horizontal stress $\sigma_H = 12.7$–14.8 MPa, minor horizontal stress $\sigma_h = 12.4$ MPa and pore pressure $u = 4.9$ MPa. Typical

✉ Malik Belmokhtar
malik.belmokhtar@enpc.fr

[1] Laboratoire Navier/CERMES, Ecole des Ponts ParisTech, 6-8 av. B. Pascal, 77455 Marne la Vallée, France

[2] Andra, Bure, France

[3] Present Address: LEMTA, Université de Lorraine, Nancy, France

characteristics of the COx claystone are a very low permeability (in order of 10^{-20} m^2) (Escoffier 2002; Davy et al. 2007; Zhang 2011; Menaceur et al. 2015, 2016), a good ability to retain radionuclides and a low diffusion coefficient resulting in very slow solute transfer.

To optimize the design of the galleries and disposal cells of a possible geological waste repository in the COx claystone, various investigations have been carried out to explore its hydromechanical behavior (Chiarelli 2000; Chiarelli et al. 2003; Zhang and Rothfuchs 2004; Hoxha et al. 2007; Hu et al. 2014; Menaceur et al. 2015, 2016). As quoted by Menaceur et al. (2015), the variability observed in published data can be linked to the different experimental procedures adopted by the different research groups involved, with respect to the state of saturation of the specimens and to the drainage conditions imposed during triaxial testing. The significant sensitivity of claystones to changes in water content has been observed by Zhang et al. (2012), Pham et al. (2007), Valès et al. (2004), Zhang and Rothfuchs (2004) and Chiarelli et al. (2003), with larger strength at lower degrees of saturation. The importance of adopting short drainage length to ensure good saturation (under stress conditions close to the in situ ones) within a reasonable period of time (no longer than one week) has been demonstrated by Monfared et al. (2011a). Actually, short drainage length ensured satisfactory drainage conditions with homogeneous pore pressure field within the specimens, allowing to investigate the intrinsic response of low-porosity specimens through fully drained tests with no excess pore pressure. In this regard, Monfared et al. (2011a) developed a new hollow cylinder triaxial apparatus with a drainage length of 10 mm. Hu et al. (2014) also tested small-sized triaxial specimens (20 mm in diameter and 40 mm in height). The failure criteria obtained on COx specimens by Hu et al. (2014) on fully saturated and fully drained specimens appeared to be compatible with that obtained on the hollow cylinder apparatus by Menaceur et al. (2015) on specimens of comparable porosity. Imperfect saturation and drainage conditions are known to overestimate the mechanical characteristics (larger stiffness and larger failure stress).

Rather few studies addressed the poroelastic response of claystones (Vincké et al. 1998; Escoffier 2002; Bemer et al. 2004; Noiret et al. 2011). Existing data show that various values of the unjacketed modulus K_s (i.e., modulus of the solid phase) have been found, resulting in a large range of possible values of Biot effective stress coefficient b, between 0.33 and 0.95 (Escoffier 2002). This variability is due to several reasons: natural variability of the samples (mineralogy, water content, porosity, etc.), coring and trimming procedures, testing protocols adopted with respect to saturation, drainage procedure. Currently, the reference value of Biot coefficient adopted by Andra in numerical calculations is most often taken equal to 0.6 (Gens et al. 2007; Charlier et al. 2013). However, because of this incertitude, it seems necessary to further investigate the poroelastic behavior of the COx claystone so as to provide more reliable values of the poroelastic parameters and to reduce their variability for poroelastic calculations. To do so, a special isotropic compression cell developed by Tang et al. (2008) and adapted by Mohajerani et al. (2012) was used and further developed in this work. In this device, a reduced drainage length (10 mm) is ensured by using a 10-mm-thick specimen drained at bottom. A high-precision local strain measurement device was developed to allow a precise determination of the poroelastic parameters of the Callovo–Oxfordian claystone along various hydromechanical loading paths.

2 Poroelasticity Framework

The Callovo–Oxfordian claystone is known as being transversely isotropic like many clayey sediments, with a preferential average orientation of the clay particles along a bedding plane that can be observed in scanning electron microscopy (e.g., Menaceur 2014). The samples tested in this work have been cored perpendicular to the bedding planes. The anisotropic properties of the COx claystone have been detected in particular by Chiarelli (2000), Escoffier (2002), Andra (2005), Mohajerani et al. (2012), Zhang et al. (2012). Typically, the axial stiffness is larger than radial one. Zhang et al. (2012) performed a series of mini-compression tests on samples parallel and perpendicular to bedding planes under different relative humidities (RH). They observed a significant structural anisotropy reflected by a ratio of Young moduli E_2/E_1 (with E_2 and E_1 parallel and perpendicular to bedding, respectively) varying between 1.6 and 1.9 (increasing with decreasing RH). The Young moduli measured at RH = 98% of are $E_1 = 1.3$ GPa and $E_2 = 2.2$ GPa, respectively. Note that these values are smaller than the values currently used in numerical simulations with E taken equal to 4 GPa (Gens et al. 2007; Charlier et al. 2013). As a consequence, an anisotropic response can be expected from the isotropic compression paths planned in this work, as observed by Noiret et al. (2011) on another claystone, the Tournemire shale.

Anisotropic poroelasticity has been considered by several authors, including Thompson and Willis (1991), Detournay and Cheng (1993), Cheng (1997), Zimmerman (2000), Ghabezloo and Hemmati (2011). The generalized Hooke's law for a porous material is given by the relation $\underline{\varepsilon} = \underline{\underline{C}}^{-1}(\underline{\sigma} - \underline{b}u)$ (Cheng 1997) where $\underline{b}$ is the Biot coefficients tensor and $\underline{\underline{C}}^{-1}$ the compliance tensor for a transverse isotropic material:

$$\begin{pmatrix} \mathrm{d}\varepsilon_1 \\ \mathrm{d}\varepsilon_2 \\ \mathrm{d}\varepsilon_2 \end{pmatrix} = \begin{pmatrix} \frac{1}{E_1} & \frac{-\nu_{12}}{E_1} & \frac{-\nu_{12}}{E_1} \\ \frac{-\nu_{12}}{E_1} & \frac{1}{E_2} & \frac{-\nu_{23}}{E_2} \\ \frac{-\nu_{12}}{E_1} & \frac{-\nu_{23}}{E_2} & \frac{1}{E_2} \end{pmatrix} \begin{pmatrix} \mathrm{d}\sigma_1 - b_1\mathrm{d}u \\ \mathrm{d}\sigma_2 - b_2\mathrm{d}u \\ \mathrm{d}\sigma_2 - b_2\mathrm{d}u \end{pmatrix} \quad (1)$$

In the case of a transverse isotropic material submitted to an isotropic stress increment ($\mathrm{d}\sigma_1 = \mathrm{d}\sigma_2 = \mathrm{d}\sigma_3 = \mathrm{d}\sigma$) the stress–strain relation can be written in the following form:

$$\mathrm{d}\varepsilon_1 = \frac{1}{E_1}(\mathrm{d}\sigma - b_1\mathrm{d}u) - \frac{2\nu_{12}}{E_1}(\mathrm{d}\sigma - b_2\mathrm{d}u) \quad (2)$$

$$\mathrm{d}\varepsilon_2 = -\frac{\nu_{12}}{E_1}(\mathrm{d}\sigma - b_1\mathrm{d}u) + \frac{(1-\nu_{23})}{E_2}(\mathrm{d}\sigma - b_2\mathrm{d}u) \quad (3)$$

in which the x_1 axis is taken perpendicular to bedding with x_2 and x_3 parallel to bedding. E_1 is the Young modulus along direction x_1 and ν_{12} the Poisson ratio in the (x_1, x_2) plane. E_2 and ν_{23} are defined in a similar fashion. For symmetry reasons, the Young moduli and Poisson ratios verify the relation $\nu_{12}/E_1 = \nu_{21}/E_2$.

The determination of the poroelastic parameters of the COx claystone was done here by performing isotropic drained, undrained and unjacketed compression tests together with pore pressure loading tests, i.e., change in pore pressure under constant confining pressure (Ghabezloo et al. 2008). In transverse isotropic materials, the changes in axial and radial strains under isotropic loading are different, leading to the definition of two moduli for axial and radial strains from relations (2) and (3), respectively.

In a drained isotropic compression test where pore pressure is kept constant ($\mathrm{d}u = 0$), the moduli, called D_1 and D_2 along directions x_1 and x_2, respectively, are given by:

$$\frac{1}{D_1} = \frac{\mathrm{d}\varepsilon_1}{\mathrm{d}\sigma} = \frac{1}{E_1}(1 - 2\nu_{12}) \quad (4)$$

$$\frac{1}{D_2} = \frac{\mathrm{d}\varepsilon_2}{\mathrm{d}\sigma} = -\frac{\nu_{12}}{E_1} + \frac{(1-\nu_{23})}{E_2} \quad (5)$$

The moduli measured in a test in which pore pressure is changed under constant confining pressure, $\mathrm{d}\sigma = 0$) are called H_1 and H_2 along directions x_1 and x_2, respectively:

$$\frac{1}{H_1} = \frac{\mathrm{d}\varepsilon_1}{\mathrm{d}u} = -\frac{b_1}{E_1} + 2\nu_{12}\frac{b_2}{E_1} \quad (6)$$

$$\frac{1}{H_2} = \frac{\mathrm{d}\varepsilon_2}{\mathrm{d}u} = \frac{\nu_{12}}{E_1}b_1 - \frac{(1-\nu_{23})}{E_2}b_2 \quad (7)$$

In an unjacketed compression test (where $\mathrm{d}\sigma = \mathrm{d}u$) moduli S_1 and S_2 in directions x_1 and x_2, respectively, are given by:

$$\frac{1}{S_1} = \frac{\mathrm{d}\varepsilon_1}{\mathrm{d}\sigma} = \frac{1}{E_1}((1-b_1) - 2\nu_{12}(1-b_2)) \quad (8)$$

$$\frac{1}{S_2} = \frac{\mathrm{d}\varepsilon_2}{\mathrm{d}\sigma} = -\frac{\nu_{12}}{E_1}(1-b_1) + \frac{(1-\nu_{23})}{E_2}(1-b_2) \quad (9)$$

An undrained isotropic compression test, carried out by closing the valves of the drainage system and by measuring the change in pore pressure u with respect to changes in the confining pressure σ, provides the Skempton coefficient $B = \mathrm{d}u/\mathrm{d}\sigma$ (Skempton 1954). The undrained moduli U_1 and U_2 in directions x_1 and x_2, respectively, are given by:

$$\frac{1}{U_1} = \frac{\mathrm{d}\varepsilon_1}{\mathrm{d}\sigma} = \frac{1}{E_1}((1-b_1B) - 2\nu_{12}(1-b_2B)) \quad (10)$$

$$\frac{1}{U_2} = \frac{\mathrm{d}\varepsilon_2}{\mathrm{d}\sigma} = -\frac{\nu_{12}}{E_1}(1-b_1B) + \frac{(1-\nu_{23})}{E_2}(1-b_2B) \quad (11)$$

In a purpose of simplicity, the transverse isotropic poroelastic framework can be degraded into an isotropic one so as to provide equivalent isotropic parameters that are useful to conduct isotropic poroelastic calculations, like, for example, in Gens et al. (2007). Adopting $E_1 = E_2$ and $\nu_{i,j} = \nu$, one gets the standard isotropic poroelastic equations:

$$\mathrm{d}\varepsilon_\mathrm{v} = -\frac{\mathrm{d}V}{V_0} = \frac{1}{K_\mathrm{d}}\left[\mathrm{d}\sigma - \mathrm{d}u + \frac{K_\mathrm{d}}{K_\mathrm{s}}\mathrm{d}u\right] = \frac{1}{K_\mathrm{d}}(\mathrm{d}\sigma - b\mathrm{d}u) \quad (12)$$

where

- K_d is the equivalent isotropic drained bulk modulus;

$$\frac{1}{K_\mathrm{d}} = -\frac{1}{V_0}\left(\frac{\partial V}{\partial \sigma_\mathrm{d}}\right)_\mathrm{u} = \frac{1}{D_1} + \frac{2}{D_2} \quad (13)$$

- b is the equivalent isotropic scalar Biot effective stress coefficient defined by:

$$b = 1 - \frac{K_\mathrm{d}}{K_\mathrm{s}} \quad (14)$$

- K_s is the unjacketed modulus:

$$\frac{1}{K_\mathrm{s}} = -\frac{1}{V_0}\left(\frac{\partial V}{\partial u}\right)_{\sigma_\mathrm{d}} = \frac{1}{S_1} + \frac{2}{S_2} \quad (15)$$

- H is the equivalent isotropic Biot modulus determined in a pore pressure loading test carried out under constant confining pressure, given by:

$$\frac{1}{H} = \frac{1}{V_0}\left(\frac{\partial V}{\partial u}\right)_\sigma = \frac{1}{H_1} + \frac{2}{H_2} = \frac{b}{K_\mathrm{d}} = \frac{1}{K_\mathrm{d}} - \frac{1}{K_\mathrm{s}} \quad (16)$$

Equation (16) shows that, knowing the drained modulus K_d, the determination of H provides an indirect evaluation of both the Biot coefficient b and the unjacketed modulus K_s.

The isotropic equivalent undrained bulk modulus K_u is given by:

$$\frac{1}{K_u} = -\frac{1}{V_0}\left(\frac{dV}{d\sigma}\right)_{m_f} = \frac{1}{U_1} + \frac{2}{U_2} \quad (17)$$

By replacing $du = B\, d\sigma$ in Eq. (12) leads to the following expression of K_u:

$$K_u = \frac{K_d}{1 - bB} \quad (18)$$

The experimental program followed in this work is based on the previous set of equations. It aims at characterizing various poroelastic parameters by running different tests so as to examine the compatibility between the results obtained, in an aim to get satisfactory confidence in the experimental determination of the poroelastic parameters.

3 Materials and Methods

3.1 The Callovo–Oxfordian Claystone

The mineralogical composition of the COx claystone, and more specifically the clay and carbonate contents, varies with depth. The total porosity is estimated between 14% in carbonated levels and 19.5% in more argillaceous levels (Yven et al. 2007). At the level of the Bure URL, the COx claystone is made up of a clay matrix (45–50% clay fraction) in which are embedded 20–30% carbonates, 20–30% quartz and a small fraction of feldspar. The clay fraction is composed of 10–24% mixed layer illite/smectite, 17–21% illite, 3–5% kaolinite, 2–3% chlorite (Gaucher et al. 2004). The smectite fraction of the mixed layer illite/smectite is estimated between 50 and 70%. It provides to the COx claystone some swelling properties (e.g., Mohajerani et al. 2012; Delage et al. 2014) and interesting self-sealing capabilities (Davy et al. 2007; Zhang 2011; Menaceur et al. 2015).

The specimens tested in this study (EST31912c and EST31912e) come from 80-mm-diameter cores that were extracted at the depth of the Bure URL (490 m). Two specimens of 38 mm diameter and 10 mm height were cored by using a diamond core in the direction perpendicular to the bedding plane and cut at the required length by using a diamond saw. The water content was obtained by weighing the sample before and after oven-drying at 105 °C during 48 h. The sample volume was determined by hydrostatic weighing to calculate the total connected porosity and the initial degree of saturation. The specimen EST31912c was tested immediately after coring. Its initial water content was equal to 7.45%, corresponding to a degree of saturation of 94.2%, considering a particle density of 2.70 g/cm^3 (Andra 2005). The specimen EST31912e, that was tested 2 months later, was preserved from evaporation by plunging it in a mix 70% paraffin, 30% vaseline oil and wrapping it in plastic film. Its water content, however, decreased to 4.54% during the conservation period, corresponding to a degree of saturation of 67.8%. The initial characteristics of the two specimens tested are presented in Table 1. A suction measurement was carried out on some cuttings of specimen EST31912c by using a chilled mirror tensiometer (WP4, Decagon), providing a value of 19.7 MPa for a specimen with a degree of saturation of 94.2%. These data are representative of a good preservation of the specimen. They are in good compatibility with the water retention curves provided by Pham et al. (2007) and Wan et al. (2013). This measurement was unfortunately not carried out on specimen EST31912e.

3.2 Experimental Device

The experimental device developed in this work is an extension of a system initially developed by Tang et al. (2008) to investigate the thermal behavior of compacted bentonites. It was further developed by Mohajerani et al. (2012) to investigate thermal pressurization in the COx claystone. As shown in Fig. 1, it is composed of a thermal isotropic compression cell connected to two pressure–volume controllers (PVC, GDS Brand) imposing pressures up to 60 MPa. Compared to previous works, the sample diameter was reduced to 38 mm in order to add a local system of axial and radial strains measurement by means of LVDTs (Fig. 1a). The short height of the sample (10 mm with drainage at bottom) results in a short drainage length that ensures a good saturation within a reasonable period of time and good drainage (see Monfared et al. (2011b)). Drainage was ensured by a thin geotextile on specimen EST31912c. To reduce the compressibility of the drainage system, the geotextile was replaced by a porous disk for specimen EST31912e. The difference between the two drainage systems (geotextile and porous disk) slightly affects the measurement of the undrained parameters. A correction of the parasite effects of the pore volume of the drainage system is presented in Appendix 2. Monfared (2011) checked the drainage performances of the geotextile under pressure. To insulate the sample from the confining fluid (silicone oil), a specially designed cylindrical neoprene membrane able to continuously envelop the top and lateral face of the sample was used, without using any piston or porous disk on the top of the sample. The membrane was tightly fixed to the bottom base by means of two O-rings.

As shown in Fig. 1b, the cell was immersed in a temperature-controlled bath. Pore pressure changes in the sample were measured by a pressure transducer (0–75 MPa

Table 1 Initial characteristics of the studied specimens

ID Ech.	w (%)	ρ (g/cm^3)	ρ_d (g/cm^3)	e	S_r (%)	(%)	Suction (MPa)
EST31912c	7.45	2.39	2.22	0.21	94.2	17.6	19.7
EST31912e	4.54	2.39	2.29	0.18	67.8	15.3	–

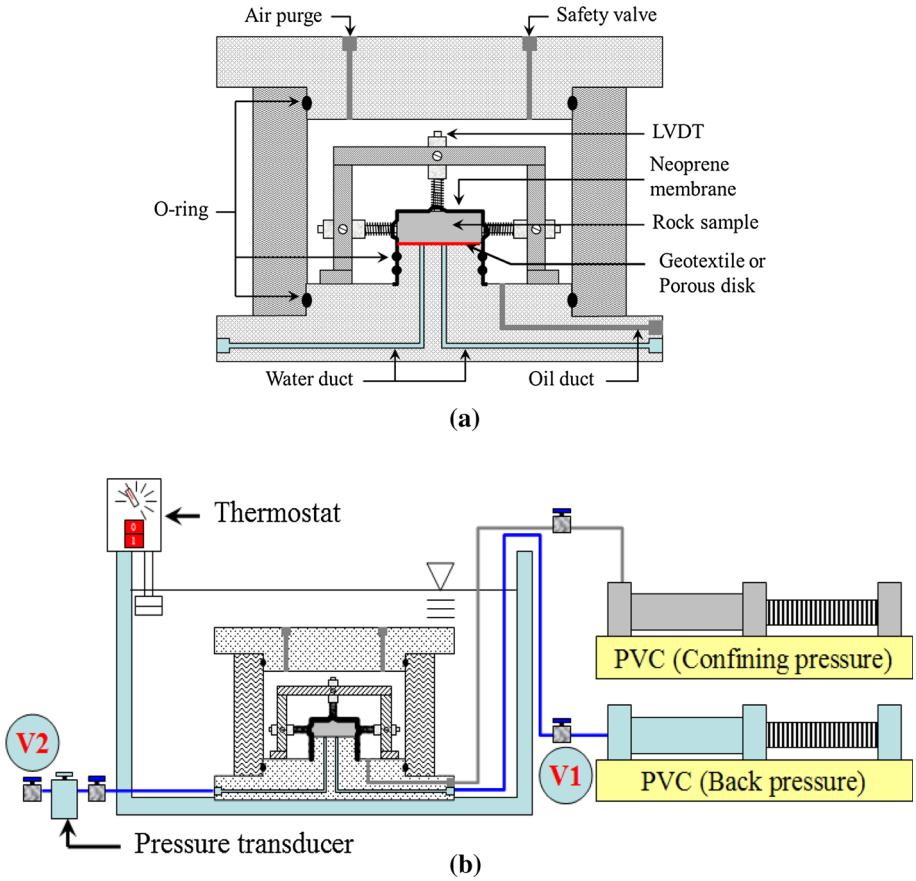

Fig. 1 **a** Isotropic compression cell; **b** overall system with controlled temperature bath

range) placed outside the bath to avoid any perturbation due to the temperature changes in the bath. The temperature of the bath was controlled with 0.1 °C accuracy and measured by means of a thermocouple. One of the two ducts arriving at the sample bottom was connected to the pressure transducer, whereas the other one was connected to the back pressure PVC. This PVC was carefully filled by demineralized and de-aired water.

3.3 Strain Measurement

The main improvement with respect to the device of Mohajerani et al. (2012) concerns the monitoring of the axial and radial strain by means of LVDTs, as shown in Fig. 2. Given the stiffness of the COx claystone, with a Young modulus of about 4000–5600 MPa (ANDRA 2005; Gens et al. 2007; Charlier et al. 2013) and because of the small size of the sample, the displacements during compression are expected to be small (around 2 µm by MPa). To avoid any disturbance due to the neoprene membrane, direct contact between the LVDT stem and the specimen was ensured by piercing the membrane with a hole smaller in diameter than the stem. Good fluid tightness was ensured by putting a drop of neoprene glue on the membrane around the stem. Using this technique, displacement measurements were improved with a minimum accuracy of 0.1 µm corresponding to a strain of 10^{-5}.

Figure 3 shows a comparison during an undrained compression test between the data of the radial LVDT in direct contact with the specimen through the membrane and that obtained by the axial one in contact with the membrane. Starting from an initial confining stress of 12 MPa with a back pressure of 4 MPa, the confining stress was increased with a loading rate of 20 kPa/min and maintained at 16.5 MPa during 13 h. Afterward, an unloading–reloading path up to a maximum pressure of 18.5 MPa was followed. Finally, the confining stress was decreased down to 12 MPa with a loading rate of 10 kPa/

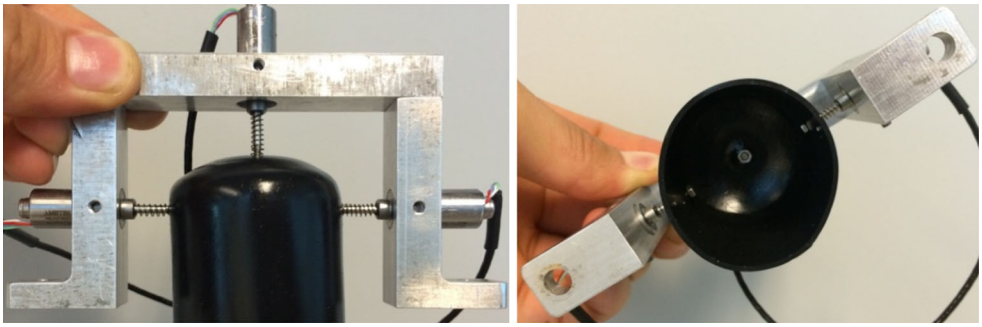

Fig. 2 Displacement measurement system

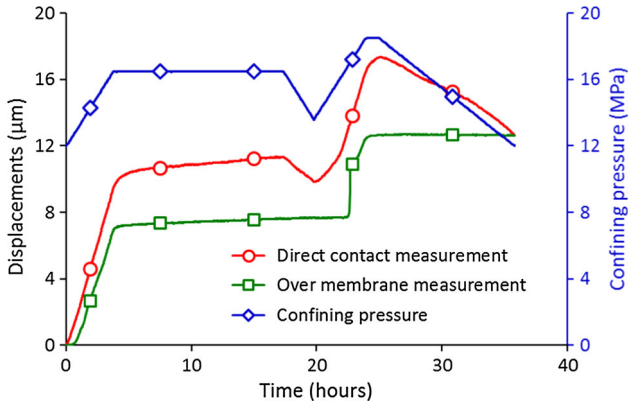

Fig. 3 Effect of the membrane on the strain measurements

min. The comparison between the two measurements clearly shows that the LVDT in direct contact with the sample precisely follows all the loading and unloading phases, while the measurements made on the membrane do not detect the unloading phases at the 18 and 26th hours. The loading sequence at 20 h is also poorly monitored. This clearly shows the improvement provided by ensuring a direct contact of the LVDT stem with the specimen through the membrane.

3.4 Saturation phase

As commented in Introduction, the mechanical properties of high clay content rocks are very sensitive to changes in water content. Given that the specimens provided to the laboratory are partially saturated (see Table 1), particular attention has been devoted to the resaturation procedure prior to mechanical testing, in an aim to limit any possible swelling. As demonstrated in swelling soils (e.g., Delage et al. (2007) and applied by Monfared et al. (2011a) on the Opalinus clay and Mohajerani et al. (2011) and Menaceur et al. (2015, 2016) on the COx claystone, it is mandatory to saturate swelling soils and clay rocks under stress conditions close to in situ one so as to minimize swelling and damage. To do so, the ducts and the geotextile were kept dry during the sample setup to avoid any contact of the sample with water. Once the sample placed on the base with the membrane put around and the cell placed and filled with the confining fluid (oil), vacuum was applied through the valve located close to the pressure transducer (valve V2 in Fig. 2) so as to evacuate any trapped air between the membrane and the sample. Then, the confining pressure was increased to 8 MPa, a value close to the in situ Terzaghi effective stress. The drainage system under vacuum was afterward filled with demineralized de-aired water through valve V2 while valve V1 was kept closed, ensuring good saturation of the drainage system. Given that evaporation and the partial desaturation of the samples resulted in a slight increase in salinity of the pore water (since dissolved salts remain within the sample pore water), saturation with demineralized water with limited swelling allows to get back to the initial salinity of the pore water.

Finally, the confining stress and pore pressure were simultaneously increased up to 12 MPa and 4 MPa, respectively, at a rate of 100 kPa/min to reach stress conditions close to in situ. Figure 4a shows the water exchange (i.e., the ratio of injected water ΔV_w monitored by the PVC with respect to the initial sample volume V_0) together with the volumetric strains measured by the LVDTs in tests EST31912c. The sample exhibits a small swelling (0.05%, at the limit of the precision of the PVC) with axial swelling larger than radial one. The monitoring of water exchanges does not seem to be satisfactory during the first day, but a good compatibility of the volume changes with water exchanges is observed after one day.

The response of the axial LVDT is not satisfactory for sample EST31912e (Fig. 4b), and no volume change could be calculated from local strain measurement. The radial strain stabilizes after one and a half day, like in sample EST31912c, but at a value significantly larger, a possible effect of the smaller initial degree of saturation.

A possible reason of the significant difference in the swelling response is the difference in initial degrees of saturation, with values of 94.2% and 67.8%, respectively, for EST31912c and EST31912e samples. Similar

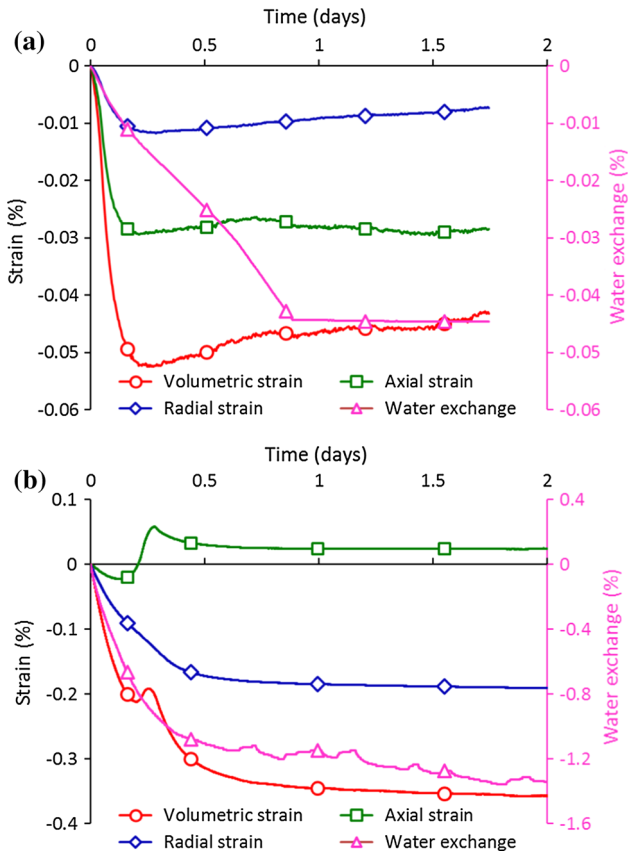

Fig. 4 Saturation phase: **a** sample EST31912c, **b** sample EST31912e

observations were made by Menaceur (2014) when testing in the oedometer two samples of COx samples with degrees of saturations of 77% and 91% and by Ewy (2015) who found larger swelling in shales and claystones with lower partial saturation. Indeed, loss of water (drying) in clayey rocks results in damage and microcracks that enhance swelling.

3.5 Loading rates

When performing a drained compression test, the pore pressure field should remain homogeneous with negligible changes in pore pressure (Gibson and Henkel 1954). Homogeneity of the pore pressure field is also mandatory when performing an unjacketed test or an undrained compression test. In practice, pore pressure can only be controlled at the sample borders connected to the drainage system. This occurs at the bottom of the 10-mm-height cylindrical specimen in the isotropic compression tests carried out here. In all cases, pore pressure homogeneity can be ensured if a sufficiently low stress rate is adopted. The loading rates depend on the sample permeability, drainage length, material's stiffness and the nature of the test carried out. It is difficult to have a perfectly homogeneous pore pressure distribution; however, a loading rate can be considered as satisfactory for a given loading path when the generated pore pressure heterogeneity inside the sample has a negligible influence on the measured strains and consequently on the evaluated poroelastic parameters (Ghabezloo et al. 2009). Some poroelastic calculations of the excess pore pressure generated during the various tests carried out in this work are presented in Appendix 1.

The calculations in Appendix 1 confirm that a loading rate of 0.5 kPa/min ensures good drainage in both the drained compression and the pore pressure loading tests. This rate was already adopted in the drained standard triaxial tests carried out by Sultan et al. (2000) on the Boom clay and by Monfared et al. (2011a) (who used a hollow cylinder triaxial cell with 10 mm drainage length) on both the Boom clay and the Opalinus clay. Calculations also show that a loading rate of 2 kPa/min is satisfactory for the unjacketed test, in which volume changes and water exchanges are smaller, given that this test mobilizes the modulus K_s of the solid phase, that is larger than the drained modulus K_d.

3.6 Correction of drainage system effect for the undrained experiments

Undrained compression tests are run by increasing the confining pressure while all valves of the drainage system are closed. The confining pressure variation results in a simultaneous change of the sample pore pressure. The measurement of the pore pressure change by the pressure transducer inevitably requires some fluid mass exchange between the pore volumes of the sample and of the drainage system. The loading rate should thus be slow enough to ensure pore pressure equilibrium between these pore volumes. Therefore, the undrained condition ($\Delta m_w = 0$) cannot be ensured in the pore volume of the sample only, and it is actually imposed in the larger volume including the pore volumes of both the specimen and the drainage and pore pressure measurement system. This artifact induces some error in the measured undrained parameters due to the compressibility of the drainage system and of the fluid filling it. A correction method should thus be applied to the measured parameters.

Wissa (1969) and Bishop (1976) were the first who proposed a correction method for the effect of the drainage system on the results of an undrained compression test, that was afterward extended to temperature effects by Ghabezloo and Sulem (2009, 2010). This correction has been applied to the results of experiments performed on Opalinus clay (Monfared et al. 2011a) and COx claystone (Mohajerani et al. 2012). The correction method is

presented in Appendix 2 along with a parametric study on the effects of various parameters.

4 Experimental program and results

The determination of the isotropic transverse parameters described in Eqs. (4)–(11) has been undertaken by running the following set of experiments:

1. A drained isotropic compression test in which the confining pressure is changed under constant pore pressure;
2. A test in which pore pressure is changed under constant total stress;
3. An unjacketed compression test in which pore pressure and confining pressure are simultaneously changed, keeping constant the Terzaghi effective stress;
4. An undrained isotropic compression test in which the confining pressure is changed while the drainage system is closed. In this test, the increase in pore pressure Δu due to an increase in confining stress $\Delta\sigma$ is measured, providing the value of the Skempton coefficient $B = \Delta u/\Delta\sigma$.

Under the simplified hypothesis of equivalent isotropy, test 1 provides the drained bulk modulus K_d, test 2 the Biot modulus H, test 3 the unjacketed modulus K_s and test 4 both the undrained bulk modulus K_u and the Skempton coefficient $B = \Delta u/\Delta\sigma$, in which Δu is the increase in pore pressure due to an increase in confining stress $\Delta\sigma$.

The experimental program was carried out under initial isotropic Terzaghi effective stresses of 10 MPa for test EST31912c and 8 MPa for test EST31912e.

4.1 Drained isotropic compression test

The drained compression test was carried out by keeping the pore pressure constant ($\Delta u = 0$) by connecting valve V1 (Fig. 1b) to the PVC controlling the pore pressure ($u = 4$ MPa). A loading rate of 0.5 kPa/min was adopted (see Appendix 1) to ensure satisfactory drained conditions with the drainage length of 10 mm. Thanks to the accuracy of the strain measurements, small stress cycles of only 500 kPa were applied, a small enough range to stay within the elastic domain (Figs. 5, 6, 7).

Three drained unloading–reloading cycles were performed, one on sample EST31912c (between 14 and 13.5 MPa) and two on sample EST31912e (between 12 and 11.6 MPa and between 12 and 11.4 MPa). The response in axial and radial strain indicates some anisotropy (Fig. 5) with smaller radial strains with ratios $\varepsilon_1/\varepsilon_2$ of 2.3 and 2.4 for samples EST31912c and EST31912e, respectively. The good repeatability observed in the two cycles carried out on sample EST31912e (Fig. 5b) provides good confidence in the results. One also observes the stress dependency of the drained compressibility, with higher modulus obtained under higher Terzaghi effective stress.

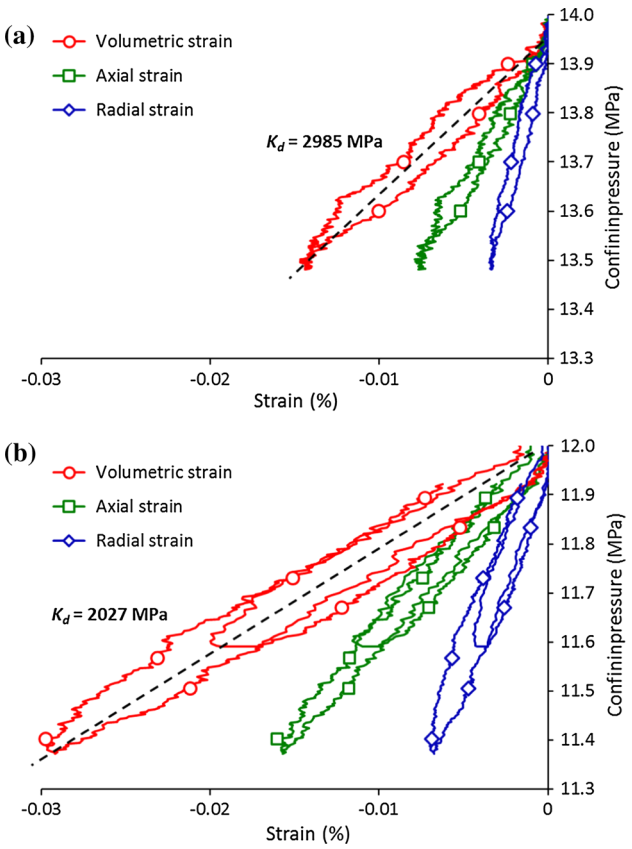

Fig. 5 Drained isotropic compression cycles: **a** EST31912c, **b** EST31912e

The anisotropic strain response provides the value of moduli D_1 and D_2 in axial and radial directions, respectively, with $D_1 = 5.6$ GPa and $D_2 = 12.8$ GPa for sample EST31912c and $D_1 = 3.7$ GPa and $D_2 = 9$ GPa for sample EST31912e.

The isotropic equivalent drained bulk modulus K_d values are equal to 2985 MPa ($\sigma_d = 14$ MPa) and 2027 MPa ($\sigma_d = 12$ MPa) for tests EST31912c and EST31912e, respectively.

4.2 Pore pressure loading test

The pore pressure loading test should be carried out under a slow rate of pressure change (0.5 kPa/mn, Appendix 1), like in a drained test, so as to ensure uniform pore pressure distribution within the sample. The pore pressure was first increased from 4 MPa up to 4.8 MPa and then decreased, resulting in an unloading–reloading cycle in Terzaghi effective stress. As previously, the pressure change was chosen small enough to remain in the elastic domain and

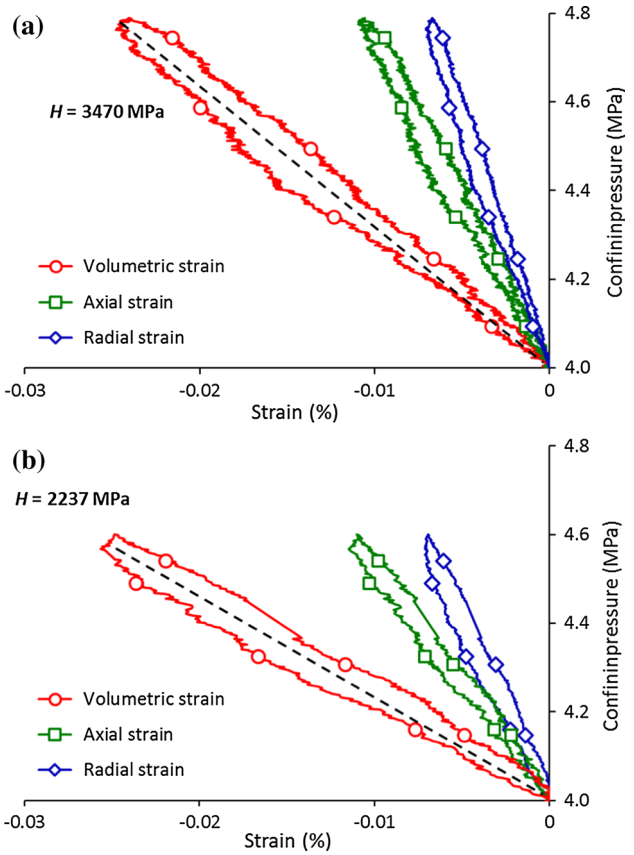

Fig. 6 Pore pressure loading–unloading test: **a** EST31912c, **b** EST31912e

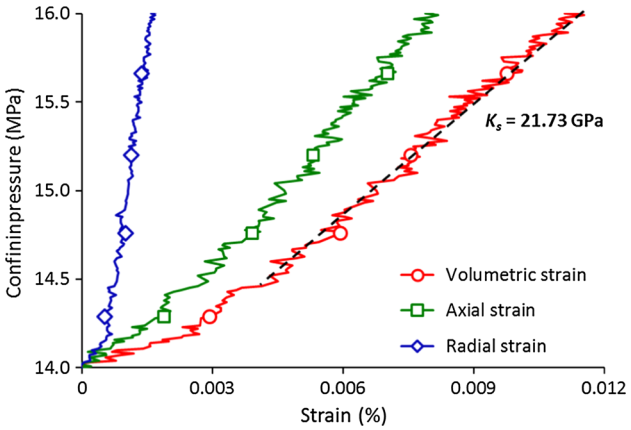

Fig. 7 Unjacketed test (EST31912c), pressure–strain response in loading phase

avoid any potential damage of the sample. As shown in Fig. 6, the response is linear and anisotropic with smaller radial strains and an anisotropy ratio $\varepsilon_1/\varepsilon_2$ of 1.8 and 1.5 for samples EST31912c and EST31912e, respectively.

The moduli H_1 and H_2 in axial and radial directions are found equal to 7.3 GPa and 13 GPa, respectively, for sample EST31912c, and to 5.2 GPa and 7.7 GPa, respectively, for sample EST31912e.

Values of equivalent isotropic Biot modulus H of 3.47 GPa under 10 MPa (test EST31912c) and of 2.237 GPa under 8 MPa (test EST31912e) are obtained (Eq. 16). Like in the drained test, one observes a stress dependency of the Biot modulus (H) with respect to Terzaghi effective stress.

4.3 Unjacketed compression test

An unjacketed compression test, in which the confining pressure and the pore pressure are increased simultaneously ($\Delta\sigma = \Delta u$, keeping the Terzaghi effective stress constant) mobilizes the compression of the solid phase, resulting in small strains that require quite a good precision in strain measurements. Moreover, the very low permeability of the COx claystone makes unjacketed compression tests rather long because of the small loading rate necessary to ensure homogeneous pore pressure field within the specimen (see Appendix 1).

The results of an unjacketed test carried out with the high-precision device of Fig. 1 on sample EST31912c at a loading rate of 2 kPa/mn are presented in Fig. 7. The isotropic confining pressure was increased from 14 MPa to 16 MPa and the pore pressure from 4 MPa to 6 MPa, keeping a constant value of the Terzaghi stress of 10 MPa. The data are presented in terms of change in axial and radial strain with respect to isotropic confining pressure. At maximum confining pressure (16 MPa) a maximum axial strain of 0.012% that corresponds to a displacement value of 0.8 µm (indicating good performance of the local strain measurement) is measured. A significantly anisotropic response is observed with radial strains (ε_2, parallel to bedding) significantly smaller than axial ones (ε_1, perpendicular to bedding) and a ratio $\varepsilon_2/\varepsilon_1$ equal to 5.7.

The isotropic equivalent unjacketed modulus obtained is equal to 21.73 GPa, corresponding to a compressibility coefficient c_s ($1/Ks$) equal to 0.046 GPa^{-1}.

4.4 Undrained compression test

The undrained compression test carried out on sample EST31912c included an unloading sequence from 13.9 down to 12.8 MPa. Four cycles were performed between 12 MPa and 11 MPa on sample EST31912e, as shown in Fig. 8 that presents the changes in radial, axial and volumetric strains with respect to the confining pressure for both tests.

Linear responses with clear anisotropy are again observed in axial and radial strains with an anisotropy ratio of 3.7 and 3.5 for tests EST31912c and EST31912e, respectively. Load cycles provide a satisfactory reversible

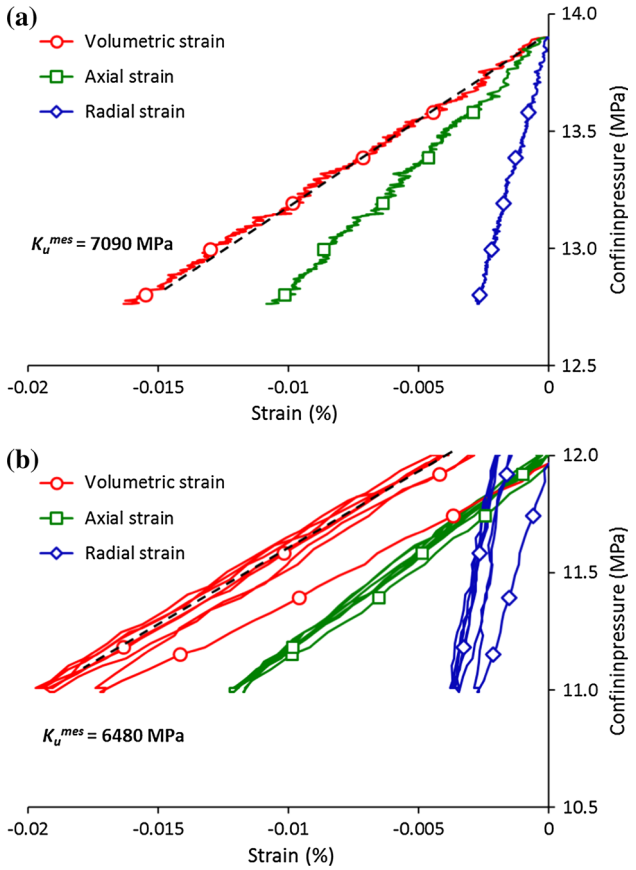

Fig. 8 Undrained isotropic compression tests: **a** EST31912c, **b** EST31912e

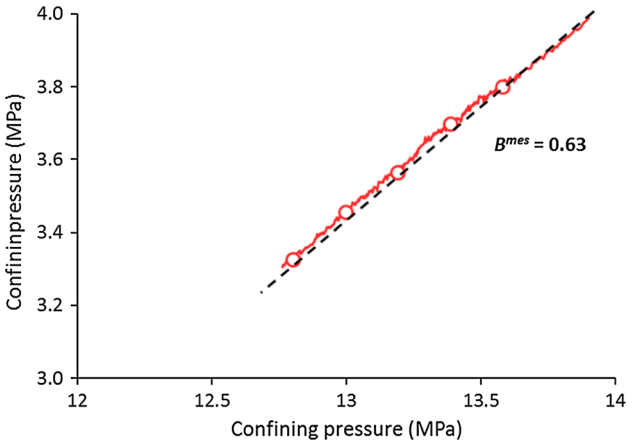

Fig. 9 Skempton coefficient measured for test EST31912c

response for the sample EST31912e (Fig. 8b). The maximum strain measured by the radial LVDTs is equal to 0.003% (10^{-5}, say a displacement of 0.52 µm) and that measured by axial LVDT is 0.011% (say a displacement of 1.09 µm), confirming the high-precision performance of the monitoring of the local strains.

The measured undrained equivalent isotropic moduli are $K_u^{mes} = 7.09$ GPa for test EST31912c and $K_u^{mes} = 6.48$ GPa for test EST31912e, respectively. They correspond to corrected values $K_u^{cor} = 12.42$ GPa and $K_u^{cor} = 10.93$ GPa, respectively. Compared to corrected values, the significantly lower measured values are due to the high ratio between the volume of the drainage system and the sample volume (V_L/V) (see Appendix 2). The smaller undrained bulk modulus in test EST31912e compared to that of test EST31912c is due to the smaller applied Terzaghi effective stress. The good correspondence between the two values provides a good confidence in the K_u values obtained.

4.4.1 Skempton Coefficient B

Figure 9 presents the changes in pore pressure with respect to the confining pressure measured on sample EST31912c when decreasing the confining stress from 14 MPa down to 12.8 MPa. The response is quite linear, and the slope provides a measured value of the Skempton coefficient $B^{mes} = 0.63$.

The correction (see Appendix 2) provides a corrected value $B^{cor} = 0.84$, with a difference compared to B^{mes} of about 25%, mostly due to the compressibility of water and to the large dead volume of the drainage system, made up of a geotextile. This corrected Skempton coefficient B^{cor} is equal to that found in the COx claystone by Mohajerani et al. (2013) in a hollow cylinder triaxial cell. These authors demonstrated that $B = 0.84$ indicated a good saturation of the specimen.

Unfortunately, a leak occurred during the test on sample EST31912e and no B value could be obtained.

5 Analysis of Experimental Results and Discussion

5.1 Biot Effective Stress Coefficients

From Eqs. (4)–(7), the Biot coefficients b_1 and b_2 can be written with respect to the measured parameters D_1, D_2, H_1, H_2 and to the unknown parameter ν_{12}, as follows:

$$b_1 = -2\nu_{12}\left[\left(\frac{\nu_{12}}{H_1}+\frac{1}{H_2}\right)\Big/\left(\frac{\nu_{12}}{D_1}+\frac{1}{D_2}\right)\right] - (1-2\nu_{12})\frac{D_1}{H_1} \tag{19}$$

$$b_2 = -\left[\left(\frac{\nu_{12}}{H_1}+\frac{1}{H_2}\right)\Big/\left(\frac{\nu_{12}}{D_1}+\frac{1}{D_2}\right)\right] \tag{20}$$

Table 2 summarizes the moduli D_1, D_2, H_1, H_2 evaluated from the drained compression and from the pore pressure test on samples EST31912c and EST31912e. The difference between the ratio D_2/D_1 and H_2/H_1 is also shown.

Table 2 Measured anisotropic modulus in drained and pore pressure tests

	EST31912c ($\sigma_d = 10$ MPa)	EST31912e ($\sigma_d = 10$ MPa)
D_1 (GPa)	5.6	3.7
D_2 (GPa)	12.8	9.0
H_1 (GPa)	−7.3	−5.2
H_2 (GPa)	−13	−7.7
D_2/D_1	2.3	2.4
H_2/H_1	1.8	1.5

Table 3 Calculation of b_1 and b_2 for different ν_{12}

ν_{12}	EST31912c ($\sigma_d = 10$ MPa)		EST31912e ($\sigma_d = 8$ MPa)	
	b_1	b_2	b_1	b_2
0.25	0.836	0.906	0.854	0.996
0.30	0.845	0.896	0.870	0.976
0.35	0.852	0.888	0.884	0.959

Now, the estimation of b_1 and b_2 is only dependent of the unknown parameter ν_{12}. The calculated values of b_1 and b_2 when ν_{12} is varied between two values considered as reasonable boundaries (0.25 and 0.35) are presented in Table 3.

One can see that the calculated values of b_1 and b_2 show a weak dependency with respect to the changes in ν_{12}. Actually, the parameter ν_{12} could be measured by a triaxial shearing test, not planned in the present experimental program carried out in an isotropic compression cell. Note, however, that Menaceur et al. (2015) obtained a ν_{12} value of 0.30 on the Callovo–Oxfordian claystone whereas Homand et al. (2006) provided a value of 0.35.

Adopting a value of 0.3 for ν_{12} provides values of $b_1 = 0.845$ and $b_2 = 0.896$ under 10 MPa Terzaghi effective stress on specimen EST31912c and of $b_1 = 0.870$ and $b_2 = 0.976$ under 8 MPa on specimen EST31912e. b_i parameters are smaller under lower stress, but specimen EST31912e, with smaller degree of saturation, is probably more damaged, another reason of having a smaller b value (Aublivé-Conil 2003).

5.2 Effect of Anisotropy on the Unjacketed Modulus

Figure 7 shows a significant anisotropy in the response of the unjacketed test, with a ratio $\varepsilon_1/\varepsilon_2$ of 5.7, indicating a compressibility perpendicular to bedding significantly larger than that parallel to bedding. This ratio is actually the highest one observed in all the tests carried out in this work.

The relation between the unjacketed modulus and the compressibility of the solid phase is complex in the case of composite materials and natural rocks made up of various minerals. The unjacketed modulus is an overall response depending on the one hand on the response in compression of the elementary particles and on the other hand on the way particles are organized together, i.e., on the fabric (or texture). It has been shown that most minerals (including quartz and calcite) exhibit a significant anisotropy with a dependence of the elastic modulus with respect to the direction (Bass 1995). This is suspected to be also true for clays platelets (and more particularly for the smectite phase) with a significant effect of adsorbed water molecules along the smectite faces, that should increase the compressibility when compression is carried out perpendicular to the platelets (i.e., perpendicular to bedding). Note that an isotropic overall response in unjacketed test with comparable axial and radial strains can be observed in sandstone for instance (Coyner 1984), when elementary grains (with anisotropic response) can be randomly oriented within the rock fabric, thanks to their rounded shape. This is obviously not the case of the fabric of the COx claystone where calcite, quartz and other detritic grains are embedded in a clay matrix (50%). In this case, the anisotropic response of the solid phase that is mobilized during an unjacketed test results from the combined response of the clay matrix and of the embedded grains. The response of the matrix itself results from both the anisotropic response of the elementary clay platelets (mixed layered illite–smectite) and their preferred orientation along the bedding plane.

5.3 Overall Compatibility of the Equivalent Isotropic Parameters

The compatibility of the set of equivalent isotropic poroelastic parameters determined from the various tests is now examined, following the approach of Ghabezloo et al. (2008) on a hardened cement paste.

The unjacketed modulus K_s directly evaluated from the unjacketed test ($K_s = 21.73$ GPa, see Fig. 7) can also be calculated indirectly from the values of the drained bulk modulus (K_d) and the Biot modulus (H) using Eq. (16). As shown in Table 4, the indirectly evaluated K_s values for both samples are very close to that measured in the unjacketed test. As expected, the values of K_d and H are stress dependent but they finally provide comparable (not stress dependent) values of K_s. This analysis shows the compatibility of the results of drained, unjacketed and pore pressure loading tests.

The isotropic equivalent Biot effective stress coefficient b can be determined by using the various poroelastic relations presented below (21a–c) by combining the results of two tests among the four performed tests (drained, undrained, unjacketed compression and pore pressure

loading tests). Expressions (21)-*d* and (21)-*e* use the results of all tests to evaluate the coefficient *b*. Note, however, that equations (c) and (d) cannot be used for sample EST31912e since the Skempton coefficient could not be measured.

$$b = \begin{cases} \dfrac{K_d}{H} & (a) \\ 1 - \dfrac{K_d}{K_s} & (b) \\ \dfrac{1}{B}\left(1 - \dfrac{K_d}{K_u}\right) & (c) \\ \dfrac{K_u}{BK_u + H} & (d) \\ \dfrac{K_u(K_s - K_d)}{K_s(K_u - K_d) + H(K_s - K_d)} & (e) \end{cases} \quad (21)$$

The Biot effective stress coefficients b calculated using the various expressions (21) are given in Table 5. One can see a good compatibility between the calculated values which vary between 0.84 and 0.89 with an average value of 0.87 for sample EST31912c and between 0.90 and 0.91 with an average value of 0.91 for sample EST31912e. Again, good overall compatibility of the set of poroelastic parameters of the COx claystone determined from the distinct performed tests is observed, with a stress dependency of the *b* coefficient (0.87 under $\sigma = 12$ MPa and 0.91 under $\sigma = 12$ MPa). This analysis shows again the overall compatibility between all the experiments and provides confidence in the parameters determined. One can then calculate the Skempton coefficient for sample EST31912e, providing a value of 0.90 using relation (14*c*).

5.4 Discussion on the Equivalent Isotropic Biot Coefficient

This section presents a parametric study aimed at providing a range of possible values of the Biot coefficient of the intact COx claystone, considering the uncertainties that affect the Young modulus, the anisotropy ratio and the unjacketed modulus of the rock. Indeed, the specimens investigated in the laboratory may have supported some damage due to the effects or coring, stress release, evaporation, trimming and resaturation under in situ stress prior to laboratory testing. These effects are suspected to weaken the mechanical properties of the tested COx specimens, that might be smaller than the intact values that govern the in situ response of the claystone mass around the waste disposal.

The elastic parameters recommended by Andra (2005) and adopted by Gens et al. (2007) and Charlier et al. (2013) (Young modulus $E = 4$ GPa and Poisson ratio $v = 0.3$) provide an isotropic equivalent drained bulk modulus $K_d = 3.3$ GPa, larger than the 2.027 GPa value determined in this study. Using Eq. (14) with $K_s = 21.7$ GPa, an equivalent isotropic *b* value of 0.85 is obtained.

To account for the uncertainties in the values of Young modulus *E* and of anisotropy ratio E_2/E_1, a parametric study was performed varying *E* between 2.5 and 4 GPa with E_2/E_1 equal to 1, 1.2, 1.6 and 2. Constant Poisson ratios $(v_{12} = v_{23} = 0.3)$ are adopted for the sake of simplicity.

The bulk modulus is calculated as follows:

$$\frac{1}{K_d} = \frac{1 - 2v_{12}}{E_1} + \frac{2(1 - v_{12} - v_{23})}{E_2} \quad (22)$$

The changes in Biot coefficient with respect to the different parameter values adopted are summarized in Table 6. Based on the range of Young modulus and anisotropy ratio adopted, the calculated drained bulk modulus K_d varies between 2.1 and 5.0 GPa, with the smallest value obtained in the isotropic case with the lowest Young modulus (2.5 GPa), also providing the largest *b* value (0.9). The largest K_d value is obtained with largest Young modulus (4 GPa) and anisotropy ratio ($E_2/E_1 = 2$), naturally providing the smallest Biot coefficient ($b = 0.77$).

The average value obtained in this study ($b = 0.91$) under stress conditions close to in situ ($\sigma_d = 8$ MPa) on extracted specimens tested in the laboratory is of course included between the minimum (0.77) and maximum (0.91) values calculated in Table 6. The results of the parametric study carried out here confirms that the perturbations and damage supported by the specimens tested in the laboratory might tend to underestimate the real COx stiffness (observed through smaller values of E_1 and K_d), resulting in an overestimation of the Biot coefficient compared to the real one. The data of Table 6 also indicate that 0.77 seems to be a reasonable lower bound for the Biot coefficient of the COx claystone.

Table 4 Calculated K_s from measured K_d and *H*

	EST31912c ($\sigma_d = 10$ MPa) (GPa)	EST31912e ($\sigma_d = 8$ MPa) (GPa)
Measured K_d (Fig. 5)	2.985	2.027
Measured *H* (Fig. 6)	3.47	2.237
Calculated K_s	21.357	21.592
Measured K_s (Fig. 7)	21.73	

Table 5 Calculation of the Biot effective stress coefficient b

		EST31912c ($\sigma_d = 10$ MPa)	EST31912e ($\sigma_d = 8$ MPa)
Unjacketed modulus K_s		21.73 GPa	
Drained modulus K_d		2.985 GPa	2.027 GPa
Biot modulus H		3.470 GPa	2.237 GPa
Undrained modulus K_u		12.424 GPa	10.931 GPa
Skempton coefficient B		0.84	–
Biot coefficient b	(a)	0.86	0.91
	(b)	0.85	0.90
	(c)	0.91	–
	(d)	0.89	–
	(e)	0.86	0.91
Mean Biot coefficient b		0.87	0.91

Table 6 Variation of the Biot coefficient

E_1 (GPa)	E_2/E_1	K_d (GPa)	Biot coefficient b
2.4	1	2.1	0.91
	1.2	2.3	0.90
	1.6	2.8	0.88
	2	3.1	0.86
4	1	3.3	0.85
	1.2	3.8	0.83
	1.6	4.4	0.80
	2	5.0	0.77

6 Conclusion

The values of the poroelastic parameters of the Callovo–Oxfordian claystone are still debated with published values of equivalent isotropic Biot coefficients comprised between 0.3 and 1.0, with an average value of 0.6 generally adopted in numerical simulations. To provide further information on parameters that are of great importance in the hydromechanical modeling in the close field around deep geological repository of radioactive waste, an experimental program was conducted in a specially designed isotropic compression cell. High-precision strain measurements were made possible by getting rid of the parasite effects of the rubber membrane. To do so, direct contact through the membrane between the LVDTs stem and the specimen has been permitted, improving significantly the accuracy of the measurements of radial and axial strains. Great care was also devoted to the saturation procedure that was carried out under stress conditions close to in situ, following previous works (Monfared et al. 2011a, b, 2012; Mohajerani et al. 2013; Menaceur et al. 2015, 2016) on low permeability claystones (Callovo–Oxfordian claystone and Opalinus clay) and the Boom clay. Satisfactory drainage conditions were also ensured by adopting a small drainage length (10 mm) and low enough stress rates during isotropic compression. The parasite effects of the drainage system on the measurement of undrained parameters have also been corrected. Various poromechanical experiments have been performed with this device: drained and undrained isotropic compression tests, unjacketed compression test and pore pressure loading test.

The COx claystone exhibited a well-marked transverse isotropic response under isotropic compression with axial strains smaller radial ones. An analysis in the framework of transverse isotropic poroelasticity provided the relations between the Biot effective stress coefficients b_1 and b_2 and the Poisson ratio v_{12} and the various moduli measured in the experiments. A parametric study showed that b_1 and b_2 had a very low sensitivity with respect to changes in v_{12}, allowing a reasonable estimation of these parameters for specimens tested in the laboratory under stress conditions close to the in situ stress state with b_2 (parallel to bedding) equal to 0.976, slightly higher than b_1 (perpendicular to bedding), equal to 0.870. This difference is related to the mobilization of the layers of water molecules adsorbed along the smectite faces in the mixed layer illite–smectite platelet within the clay matrix that results in a smaller stiffness perpendicular to bedding.

The experimental results were also considered within an equivalent isotropic poroelastic framework, providing a direct determination of the equivalent isotropic poroelastic parameters of the COx claystone: drained bulk modulus K_d, undrained bulk modulus K_u, Skempton coefficient B, unjacketed modulus K_s and Biot modulus H. A very good compatibility between the results of various experiments was found, showing their quality, demonstrating the robustness of the method and giving confidence in the obtained experimental data. The results showed the stress dependency of parameters K_d, K_u and H, that increased with increased effective stress. An indirect evaluation of the unjacketed modulus K_s showed that it was not stress

dependent. For the tested specimens, cored at a depth of 490 m in the Underground Research Laboratory of Bure with around 50% clay fraction, the value of the equivalent isotropic Biot effective stress coefficient was found equal to 0.91 under a stress state close to that prevailing in situ (mean total stress of 12 MPa and pore pressure of 4 MPa).

The poroelastic parameters determined here are that of a laboratory specimen previously extracted from the rock mass and probably affected by coring, stress release, desaturation, evaporation, trimming and resaturation under in situ stresses. Given the susceptibility of claystones to damage, it is probable that these successive effects have some consequences on the parameters determined. A parametric study was hence conducted to investigate the effects of changes in Young modulus and anisotropy ratio on the b value. The possible effects of damage due to sample extraction, that results in a decrease in Young modulus, have been investigated and a range of b values between 0.77 (corresponding to the estimated real in situ value of Young modulus of 4 MPa in an isotropic case) and 0.91 (with a Young modulus decreased to 2.4 GPa and a maximum anisotropy ratio $E_1/E_2 = 2$) has been determined. This value $b = 0.77$ seems to be a reasonable lower bound for the Biot coefficient.

This work should be completed in the laboratory by poromechanical experiments under deviatoric loading to evaluate all the transverse isotropic poroelastic parameters. The variability and stress dependency of these parameters should also be further investigated.

Appendix 1: Loading Rates

In all the tests performed with controlled pore water pressure (drained test, pore pressure loading and unjacketed test), the pore water pressure field should be homogeneous within the samples. A drained compression test should be performed with no excess pore pressure (Gibson and Henkel 1954), but, as recalled by the calculations conducted by Monfared et al. (2011a), a low level of excess pore pressure may be observed even at very slow loading rate. The drained condition is considered satisfactory if the excess pore pressure is negligible with respect to the applied confining pressure.

Commonly, a rate of 0.5 kPa/min is used in drained isotropic compression test on stiff clays (e.g., Sultan et al. 2000). The calculations run by Monfared et al. (2011a) confirmed the validity of this rate in a hollow triaxial cell with a drainage length of 10 mm, equal to that adopted here. To confirm Monfared et al. (2011a) calculations, a numerical resolution of the coupled hydromechanical equations of poroelasticity was performed using the finite element method with the 2D FreeFem++ code considering an axisymmetric calculation (Hecht 2012). In a purpose of simplicity, the calculations are performed considering an isotropic material. The governing equations are recalled below:

$$\nabla \cdot \sigma + f = 0 \tag{23}$$

$$\nabla \cdot q + \frac{\partial m_f}{\partial t} = 0 \tag{24}$$

$$q = -\rho_f \frac{k}{\mu_f} \nabla \cdot p_f \tag{25}$$

$$\underline{\mathrm{d}\varepsilon} = \underline{\underline{S}}(\underline{\mathrm{d}\sigma} - b\underline{\mathrm{d}u}) \tag{26}$$

with

$$\underline{\underline{S}} = \begin{pmatrix} \frac{1}{E} & \frac{-\nu}{E} & \frac{-\nu}{E} \\ \frac{-\nu}{E} & \frac{1}{E} & \frac{-\nu}{E} \\ \frac{-\nu}{E} & \frac{-\nu}{E} & \frac{1}{E} \end{pmatrix} \tag{27}$$

$$\mathrm{d}\phi = -b\mathrm{d}\varepsilon_v + \frac{1}{N}\ \mathrm{d}u, \frac{1}{N} = \frac{b - \phi_0}{K_s} \tag{28}$$

The Young modulus E and Poisson ratio ν were taken equal to 4000 MPa and 0.3, respectively (Gens et al. 2007), providing a drained bulk modulus K_d of 3333 MPa. The unjacketed bulk modulus K_s was taken equal to 21.7 GPa (Sect. 4.1), resulting in a Biot coefficient b of 0.84 (Eq. 14). A permeability coefficient k of 20^{-20} m^2 was adopted, with a porosity ϕ of 14%, a bulk water

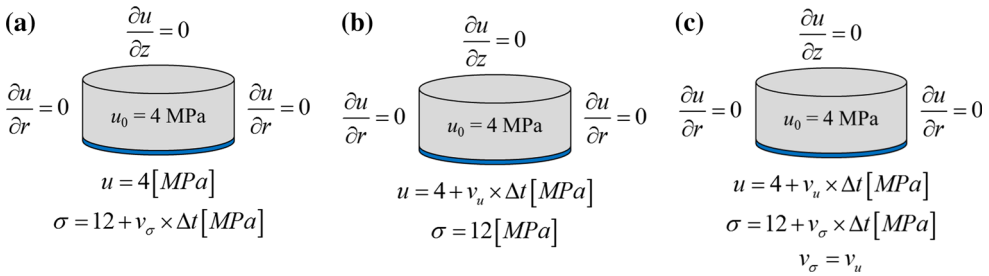

Fig. 10 Initial and boundary conditions for the different tests. **a** Drained test. **b** Pore pressure test. **c** Unjacketed test

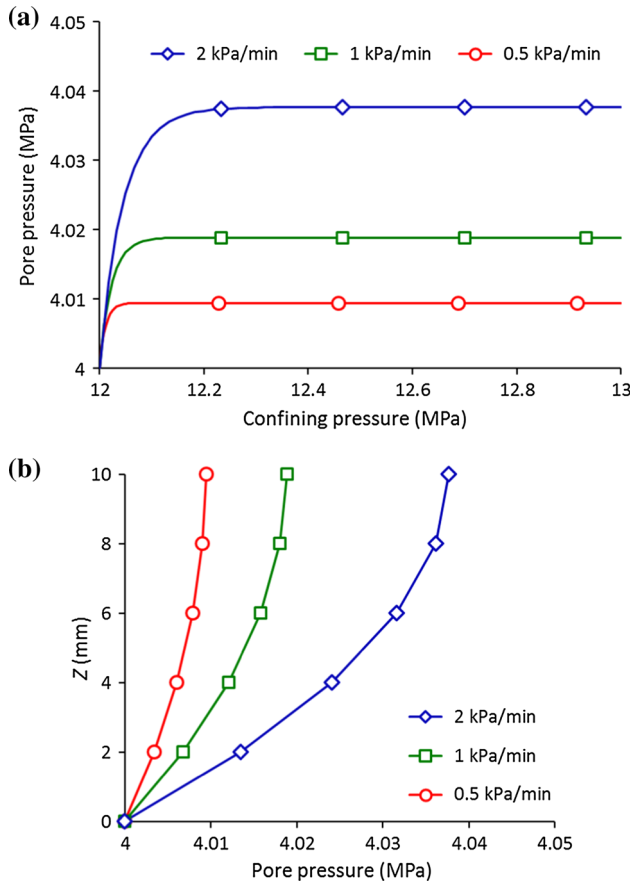

Fig. 11 Calculated pore water pressure in a drained isotropic compression test: **a** pore pressure versus confining pressure at $Z = 10$ mm, **b** calculated pore pressure along the sample at the end of loading

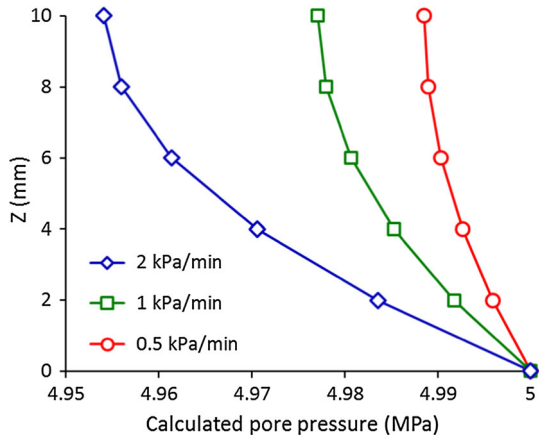

Fig. 12 Calculated excess pore pressure profile in a pore pressure test

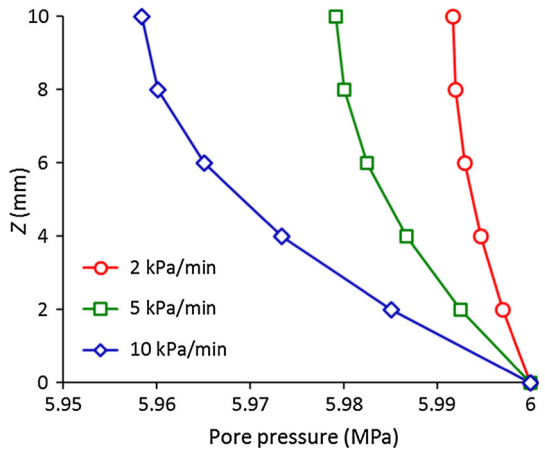

Fig. 13 Evolution of pore pressure at $z = 10$ mm with respect to confining pressure

compression modulus $K_w = 2237$ MPa and a water viscosity at 25 °C $\mu_w = 8.9 \times 10^{-10}$ MPa.s at 25 °C (Spang 2002).

The effects of changes in loading rates of total stress $v_\sigma = d\sigma/dt$ (drained isotropic compression test and unjacketed test) and pore pressure $v_u = du/dt$ (unjacketed test and pore pressure loading test) were considered in the simulations. The drained isotropic compression test was started from a confining stress of 12 MPa and a pore water pressure of 4 MPa with an applied increase in confining pressure $\Delta\sigma = 1$ MPa. The pore pressure test started from the same conditions with an applied increase in pore water pressure $\Delta u = 1$ MPa. In the unjacketed test, values of $\Delta\sigma = \Delta u = 2$ MPa were adopted. The principle of the calculations conducted and boundary conditions are presented in Fig. 10.

Drained Compression Test

The result of the simulations is presented, for all the considered loading rates (0.5, 1 and 2 kPa/min) in terms of excess pore pressure at $z = 10$ mm (the farthest point from the drainage porous disk) in Fig. 11a, and in terms of pore pressure profile in Fig. 11b. It is observed that, unsurprisingly, the lowest excess pore pressure calculated at $z = 10$ mm is obtained at the lowest rate of 0.5 kPa/min with a value of 9 kPa (obtained once the confining stress reaches 12.05 MPa), negligible with respect to the value of 4 MPa imposed at the bottom boundary. Note, however, that the value of 38 kPa obtained at 2 kPa/min is not critical and that a rate of 1 kPa/min (19 kPa excess pore pressure, with the steady state reached when the confining stress is equal to 12.10 MPa) could be satisfactory. The pore pressure profiles have a shape typical of a consolidation problem.

Pore Pressure Loading Test

Unsurprisingly, the conclusions drawn from the data of the simulations of pore pressure loading tests at all rates (0.5, 1

and 2 kPa/min, pore pressure profiles in Fig. 12) lead to the same conclusions as for the drained state, with an maximum excess pore pressure of 11 kPa at $z = 10$ mm at 0.5 kPa/min. Here also, the excess pore pressure at 2 kPa/min is smaller than 50 kPa, and it seems that tests could have been run at 1 kPa/min, with a maximum excess pore pressure of 23 kPa.

Unjacketed Compression Test

The unjacketed test was carried out by maintaining $\Delta\sigma = \Delta u$, starting from $\sigma_i = 12$ MPa and $u_i = 4$ MPa and increased up to 14 and 6 MPa, respectively. There are less water exchanges involved during unjacketed tests compared to the previous drained tests because only the compression of the solid phase is involved, with K_s larger than K_d, resulting in less sample volume changes involved.

Figure 13 shows the changes in pore pressure at $z = 10$ mm for rates of 2, 5 and 10 kPa/min. The negligible difference in pore pressure computed at 2 kPa/min at $z = 10$ mm (5.991 MPa instead of 6 MPa) shows that the pore pressure field is satisfactorily homogeneous. A difference of 20 kPa (around 0.3%) is observed at 5 kPa/min, showing that this rate could also have been adopted.

Appendix 2: Correction of the Effect of the Drainage System in Undrained Tests

The expression of the corrected Skempton coefficient (B^{cor}) with respect to the measured one (B^{mes}) is given below (Monfared et al. (2011a), following Bishop (1976)). For the sake of simplicity, the equations are written in terms of compressibility $c_i = 1/K_i$.

where V_p, V_g and V_L are the volumes of the porous disk, geotextile and connecting lines, respectively, and c_{dp}, c_{dg} and c_L their drained compressibilities. ϕ and ϕ_p are the porosities of the sample and the porous disk, respectively. V, c_d, c_u, and B are the volume, the drained compressibility, the undrained compressibility and the Skempton coefficient of the sample. c_s is the unjacketed compressibility.

The volume of samples EST31912c and EST31912e are $V = 11795$ mm^3 and $V = 13847$ mm^3, respectively. The volume of the connecting lines, porous disk and geotextile are $V_L = 2412$ mm^3, $V_p = 2268$ mm^3 and $V_g = 113$ mm^3, respectively. Monfared et al. (2011a) performed a calibration test on a dummy metal sample and found a drained compressibility of the connecting lines $c_L = 0.32$ GPa^{-1}, a drained compressibility of the porous disk $c_{dp} = 1.02$ - GPa^{-1} and a drained compressibility of the geotextile $c_{dg} = 9.33$ GPa^{-1}. The porosity of the porous disk was $\phi_p = 0.22$. The water compressibility at 25 °C is $c_w = 0.447$ GPa^{-1} (Spang 2002). The corrected undrained bulk modulus and Skempton coefficient presented in Sect. 4.4 are calculated using these parameters.

Parametric Study on the Induced Errors

A parametric study is presented here to better clarify the influence of various material and drainage system properties on the induced errors on different undrained parameters. The error on a quantity Q is evaluated as $(Q_{measured} - Q_{corrected})/Q_{corrected}$. The most influent parameters on the error are the drained compressibility c_d, the porosity ϕ and the ratio of the volume of the drainage system to the volume of the tested sample V_L/V. Three values of the drained compressibility c_d in the range of that of the COx claystone (0.1, 0.3 and 0.6 GPa^{-1}) and $c_s = 0.05$ GPa^{-1}. The

$$B^{cor} = \frac{B^{mes}}{1 + \frac{1}{V(c_d + c_s)}\left(V_p c_{dp} + V_g c_{dg} - B^{mes}\left(V_p\left(c_{dp} + \phi c_w\right) + V_g c_{dg} + V_L(c_w + c_L)\right)\right)} \tag{29}$$

The corrected undrained compressibility (c_u^{cor}) is then written as:

$$c_u^{cor} = \frac{c_d - c_u^{mes}}{1 + \frac{1}{V(c_d + c_s)}\left[V_p c_{dp} + V_g c_{dg} - \frac{V_p\left(c_{dp} + \phi_p c_w\right) + V_g c_{dg} + V_L(c_w + c_L)}{(c_d - c_s)}\left(c_d - c_u^{mes}\right)\right]} \tag{30}$$

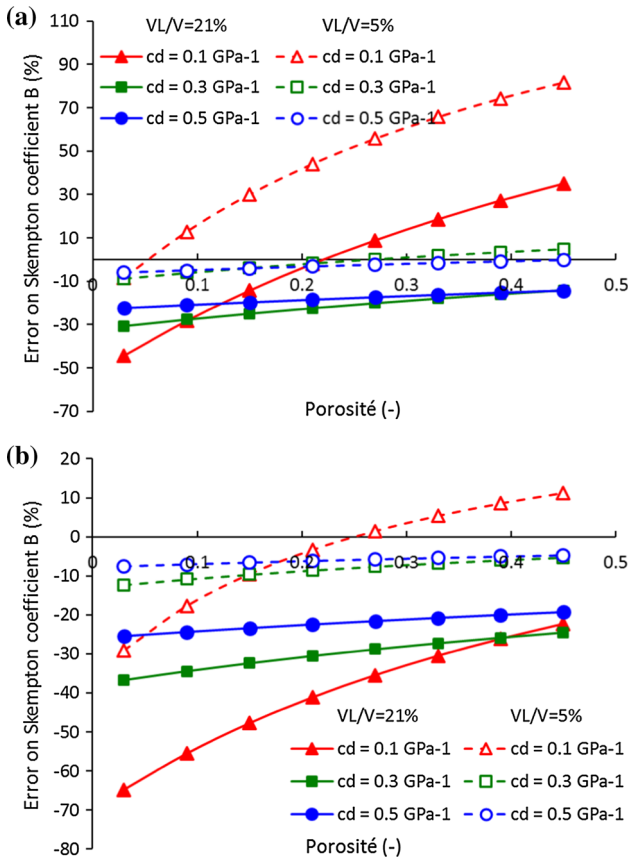

Fig. 14 Parametric study of the error on Skempton coefficient (B). **a** Geotextile. **b** Porous disk

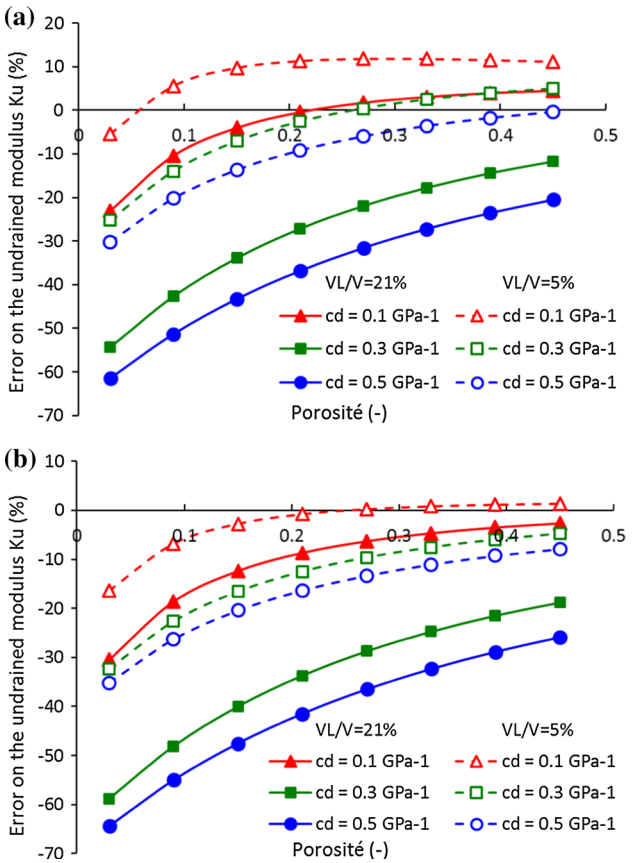

Fig. 15 Parametric study of the error on the undrained modulus (K_u)

volume ratio V_L/V was taken equal to 0.21 which corresponds to our experiment, and to further analyze the effect of the dead volume, a second ratio of 0.05 is also taken. The porosity is varied from 0.03 to 0.45.

Figure 14 shows the error on the measurement of the Skempton coefficient. When the rock is relatively highly compressible ($c_d = 0.5$ and $c_d = 0.3$ GPa^{-1}), the range of error does not vary a lot between small and high porosities. A greater volume of the drainage system underestimates the Skempton coefficient (B). The measured Skempton coefficient juggles between a slight underestimating and a slight overestimating when a geotextile is used. But with a lower compressibility, the error varies a lot as a function of the porosity. In fact, we can observe that for a volume ratio of 0.21 the Skempton coefficient is underestimated with an error of 44% in case of geotextile for 0.03 porosity and it is overestimated with an error of 35% for 0.45 porosity. When a porous disk is used, the Skempton coefficient is always underestimated (from 65 to 22%) for the same volume ratio. The error is more important and B is highly overestimated if the volume ratio is smaller on the use of geotextile and a high-porosity material.

The error made on the measurement of the undrained bulk modulus (K_u) is shown in Fig. 15. Unlike for the Skempton coefficient, the error is more important for higher compressibilities. The effect of the volume ratio is more significant in the error on the measurement of K_u, as a large difference is shown between the two volume ratios. Once more, the error induced by the use of a porous disk is slightly more important than the geotextile.

References

Andra (2005) Synthesis argile: evaluation of the feasibility of a geological repository in argillaceous formation http://www.andra.fr/download/site-principal/document/editions/266.pdf

Aublivé-Conil N (2003) Modélisation du comportement mécanique des argiles raides avec prise en compte de l'endommagement: application aux argilites de l'Est. Ph.D. thesis, Université de Cergy Pontoise

Bass JD (1995) Elasticity of minerals, glasses, and melts. In: Thomas JA (ed) Mineral physics and crystallography: a handbook of physical constants. American Geophysical Union, pp 45–63

Bemer E, Longuemare P, Vincké O (2004) Poroelastic parameters of Meuse/Haute Marne argillites: effect of loading and saturation states. Appl Clay Sci 26:359–366

Bishop AW (1976) The influence of system compressibility on the observed pore-pressure response to an undrained change in stress in saturated rock. Géotechnique 26:371–375

Charlier R, Collin F, Pardoen B, Talandier J, Radu JP, Gerard P (2013) An unsaturated hydro-mechanical modelling of two in situ experiments in Callovo–Oxfordian argillite. Eng Geol 165:46–63

Cheng AH (1997) Material coefficients of anisotropic poroelasticity. Int J Rock Mech Min Sci 34:199–205

Chiarelli AS (2000) Étude expérimentale et modélisation du comportement mécanique de l'argilite de l'est. Ph.D. thesis, Université Lille I

Chiarelli AS, Shao JF, Hoteit N (2003) Modeling of elastoplastic damage behavior of a claystone. Int J Plast 19:23–45

Coyner KB (1984) Effects of stress, pore pressure, and pore fluids on bulk strain, velocity, and permeability in rocks. Ph.D. thesis, MIT

Davy CA, Skoczylas F, Barnichon J-D, Lebon P (2007) Permeability of macro-cracked argillite under confinement: gas and water testing. Phys Chem Earth Parts A/B/C 32:667–680

Delage P, Le T-T, Tang A-M, Cui YJ, Li XL (2007) Suction effects in deep Boom clay block samples. Géotechnique 57:239–244

Delage P, Menaceur H, Tang A-M, Talandier J (2014) Suction effects in deep Callovo–Oxfordian claystone Suction effects in deep Callovo–Oxfordian claystone. Géotech Lett 4:267–271

Detournay E, Cheng AH (1993) Fundamentals of poroelasticity. In: Fairhurst C (ed) Chapter 5: Comprehensive rock engineering Prince practices project vol II, Anal Des Method, Pergamon Press II:113–171

Escoffier S (2002) Caractérisation expérimentale du comportement hydromécanique des argilites de Meuse Haute-Marne. Ph.D. thesis, Institut National Polytechnique de Lorraine

Ewy RT (2015) Shale/claystone response to air and liquid exposure, and implications for handling, sampling and testing. Int J Rock Mech Min Sci 80:388–401

Gaucher E, Robelin C, Matray JM, Négrel G, Gros Y, Heitz JF, Vinsot A, Rebours H, Cassagnabère A, Bouchet A (2004) ANDRA underground research laboratory: interpretation of the mineralogical and geochemical data acquired in the Callovian-Oxfordian formation by investigative drilling. Phys Chem Earth 29:55–77

Gens A, Vaunat J, Garitte B, Wileveau Y (2007) In situ behaviour of a stiff layered clay subject to thermal loading: observations and interpretation. Géotechnique 57:207–228

Ghabezloo S, Hemmati S (2011) Poroelasticity of a micro-heterogeneous material saturated by two immiscible fluids. Int J Rock Mech Min Sci 48:1376–1379

Ghabezloo S, Sulem J (2009) Stress dependent thermal pressurization of a fluid-saturated rock. Rock Mech Rock Eng 42:1–24

Ghabezloo S, Sulem J (2010) Effect of the volume of the drainage system on the measurement of undrained thermo-poro-elastic parameters. Int J Rock Mech Min Sci 47:60–68

Ghabezloo S, Sulem J, Guédon S, Martineau F, Saint-Marc J (2008) Poromechanical behaviour of hardened cement paste under isotropic loading. Cem Concr Res 38:1424–1437

Ghabezloo S, Sulem J, Saint-Marc J (2009) The effect of undrained heating on a fluid-saturated hardened cement paste. Cem Concr Res 39:54–64

Gibson RE, Henkel DJ (1954) Influence of duration of tests at constant rate of strain on measured "drained" strength. Géotechnique 4:6–15

Hecht F (2012) New development in freefem+. J Numer Math 20:251–265. doi:10.1515/jnum-2012-0013

Homand F, Shao JF, Giraud A, Auvray C, Hoxha D (2006) Pétrofabrique et propriétés mécaniques des argilites. Comptes rendus Géosci 338:882–891

Hoxha D, Giraud A, Homand F, Auvray C (2007) Saturated and unsaturated behaviour modelling of Meuse-Haute/Marne argillite. Int J Plast 23:733–766

Hu DW, Zhang F, Shao JF (2014) Experimental study of poromechanical behavior of saturated claystone under triaxial compression. Acta Geotech 9:207–214

Menaceur H (2014) Comportement thermo-hydro-mécanique et microstructure de l'argilite du Callovo-Oxfordien. Ph.D. thesis, Université Paris Est

Menaceur H, Delage P, Tang A-M, Conil N (2015) The thermo-mechanical behaviour of the Callovo–Oxfordian claystone. Int J Rock Mech Min Sci 78:290–303

Menaceur H, Delage P, Tang A-M, Conil N (2016) On the thermo-hydro-mechanical behaviour of a sheared callovo-oxfordian claystone sample with respect to the EDZ behaviour. Rock Mech Rock Eng 49:1875–1888

Mohajerani M, Delage P, Monfared M, Tang A-M, Sulem J, Gatmiri B (2011) Oedometric compression and swelling behaviour of the Callovo–Oxfordian argillite. Int J Rock Mech Min Sci 48:606–615

Mohajerani M, Delage P, Sulem J, Monfared M, Tang A-M, Gatmiri B (2012) A laboratory investigation of thermally induced pore pressures in the Callovo–Oxfordian claystone. Int J Rock Mech Min Sci 52:112–121

Mohajerani M, Delage P, Sulem J, Monfared M, Tang A-M, Gatmiri B (2013) The thermal volume changes of the Callovo–Oxfordian Claystone. Rock Mech Rock Eng 47:131–142

Monfared M (2011) Couplages température-endommagement-perméabilité dans les sols et roches argileux. Ph.D. thesis, Université Paris-Est

Monfared M, Delage P, Sulem J, Mohajerani M, Tang A-M, De Laure E (2011a) A new hollow cylinder triaxial cell to study the behavior of geo-materials with low permeability. Int J Rock Mech Min Sci 48:637–649

Monfared M, Sulem J, Delage P, Mohajerani M (2011b) A Laboratory Investigation on Thermal Properties of the Opalinus Claystone. Rock Mech Rock Eng 44:735–747

Monfared M, Sulem J, Delage P, Mohajerani M (2012) On the THM behaviour of a sheared Boom clay sample: Application to the behaviour and sealing properties of the EDZ. Eng Geol 124:47–58

Noiret A, Giot R, Bemer E, Giraud A, Homand F (2011) Hydromechanical behavior of Tournemire argillites: measurement of the poroelastic parameters and estimation of the intrinsic permeability by oedometric tests. Int J Numer Anal Methods Geomech 35:496–518. doi:10.1002/nag.906

Pham QT, Vales F, Malinsky L, Nguyen M-D, Gharbi H (2007) Effects of desaturation–resaturation on mudstone. Phys Chem Earth, Parts A/B/C 32:646–655

Skempton AW (1954) The pore-pressure coefficients A and B. Géotechnique 4:143–147

Spang B (2002) Excel add-in for properties of water and steam in SIunits. http://www.cheresources.com/iapwsif97.shtml

Sultan N, Delage P, Cui YJ (2000) Comportement thermomécanique de l'argile de Boom. Comptes Rendus l'Académie des Sci - Ser IIB - Mech 328:457–463

Tang A-M, Cui Y-J, Barnel N (2008) Thermo-mechanical behaviour of a compacted swelling clay. Geotechnique 58:45–54

Thompson M, Willis JR (1991) A Reformulation of the Equations of Anisotropic Poroelasticity. J Appl Mech 58:612–616

Valès F, Nguyen Minh D, Gharbi H, Rejeb A (2004) Experimental study of the influence of the degree of saturation on physical and mechanical properties in Tournemire shale (France). Appl Clay Sci 26:197–207

Vincké O, Longuemare P, Boutéca M, Deflandre J-P (1998) Investigation of the poromechanical behavior of shales in the elastic domain. Pap SPE 47589:1–6

Wan M, Delage P, Tang A-M, Talandier J (2013) Water retention properties of the Callovo–Oxfordian claystone. Int J Rock Mech Min Sci 64:96–104

Wileveau Y, Cornet FH, Desroches J, Blumling P (2007) Complete in situ stress determination in an argillite sedimentary formation. Phys Chem Earth 32:866–878

Wissa AEZ (1969) Pore pressure measurement in saturated stiff soils. J Soil Mech Found Div Am Soc Civ Eng 95(SM4):1063–1073

Yven B, Sammartino S, Geraud Y, Homand F, Villieras F (2007) Mineralogy, texture and porosity of Callovo–Oxfordian argilites of the Meuse/Haute-Marne region (eastern Paris Basin). Mémoires la société Géologique Fr 0249–7546:73–90

Zhang CL (2011) Experimental evidence for self-sealing of fractures in claystone. Phys Chem Earth 36:1972–1980

Zhang CL, Rothfuchs T (2004) Experimental study of the hydro-mechanical behaviour of the Callovo–Oxfordian argillite. Appl Clay Sci 26:325–336

Zhang F, Xie SY, Hu DW, Gatmiri B (2012) Effect of water content and structural anisotropy on mechanical property of claystone. Appl Clay Sci 69:79–86

Zimmerman RW (2000) Coupling in poroelasticity and thermoelasticity. 37:79–87